



EUROfusion

EUROFUSION WPMST1-CP(16) 15071

C Hopf et al.

Advances in Neutral Beam Current Drive Experiments on ASDEX Upgrade

Preprint of Paper to be submitted for publication in
Proceedings of 26th IAEA Fusion Energy Conference



This work has been carried out within the framework of the EUROfusion Consortium and has received funding from the Euratom research and training programme 2014-2018 under grant agreement No 633053. The views and opinions expressed herein do not necessarily reflect those of the European Commission.

This document is intended for publication in the open literature. It is made available on the clear understanding that it may not be further circulated and extracts or references may not be published prior to publication of the original when applicable, or without the consent of the Publications Officer, EUROfusion Programme Management Unit, Culham Science Centre, Abingdon, Oxon, OX14 3DB, UK or e-mail Publications.Officer@euro-fusion.org

Enquiries about Copyright and reproduction should be addressed to the Publications Officer, EUROfusion Programme Management Unit, Culham Science Centre, Abingdon, Oxon, OX14 3DB, UK or e-mail Publications.Officer@euro-fusion.org

The contents of this preprint and all other EUROfusion Preprints, Reports and Conference Papers are available to view online free at <http://www.euro-fusionscipub.org>. This site has full search facilities and e-mail alert options. In the JET specific papers the diagrams contained within the PDFs on this site are hyperlinked

Advances in Neutral Beam Current Drive Experiments on ASDEX Upgrade

C. Hopf¹, D. Rittich¹, B. Geiger¹, A. Bock¹, A. Burckhart¹, R. McDermott¹, A. Mlynek¹, C. Rapson¹, M. Reich¹, F. Ryter¹, M. Willensdorfer¹, the ASDEX Upgrade Team¹ and the EUROfusion MST1 Team²

¹Max-Planck-Institut für Plasmaphysik, Boltzmannstr. 2, 85748 Garching bei München

²see <http://www.euro-fusionscipub.org/mst1>

Corresponding Author: christian.hopf@ipp.mpg.de

Abstract:

A number of devices – ASDEX Upgrade (AUG) among them – have reported in the past that the fast ion and current profiles driven by off-axis neutral beam injection (NBI) appear to be broadened by microturbulent transport compared with neoclassical predictions. In this paper we show that despite a comprehensive set of relevant diagnostics on AUG the expected levels of microturbulence-induced transport of off-axis injected fast ions cannot be resolved. For on-axis beams fast ion D_α spectroscopy can resolve fast ion transport with diffusion coefficients of $0.1 \text{ m}^2/\text{s}$ or lower and for the presented discharge we find that $\sim 0.3 \text{ m}^2/\text{s}$ describes the results best, but fishbones may also contribute to fast ion transport in this discharge. The analysis substantially profited from some recent progress through accurate measurements of the actual neutral beam geometries that deviate slightly, yet significantly from the nominal geometries, and in the calibration of the Motional Stark Effect polarimetry (MSE) system.

In view of steady-state tokamak operation, discharges with 800 kA plasma current, $q_{95} = 5.5$, $q_{\min} > 1.5$, up to 12.5 MW NBI and 2.8 MW of ECRH recently achieved a two-seconds-long practically non-inductive phase with $> 40\%$ NBCD, $> 40\%$ bootstrap current, and $\sim 10\%$ ECCD and maintained their plasma current over that period with the central solenoid current set constant. These discharges provide a good benchmark for the calculated neutral beam driven current.

1 Introduction

Stationary operation of a tokamak requires complete replacement of the inductively driven plasma current by the intrinsic bootstrap current and external sources such as neutral beam current drive (NBCD) and electron cyclotron current drive (ECCD). To keep such steady-state scenarios free from confinement-degrading low m/n MHD instabilities, this current needs to be driven off axis.

In experiments on ASDEX Upgrade (AUG) that switched between on-axis and off-axis NBI the Motional Stark Effect polarimetry (MSE) time traces that monitored changes in the current

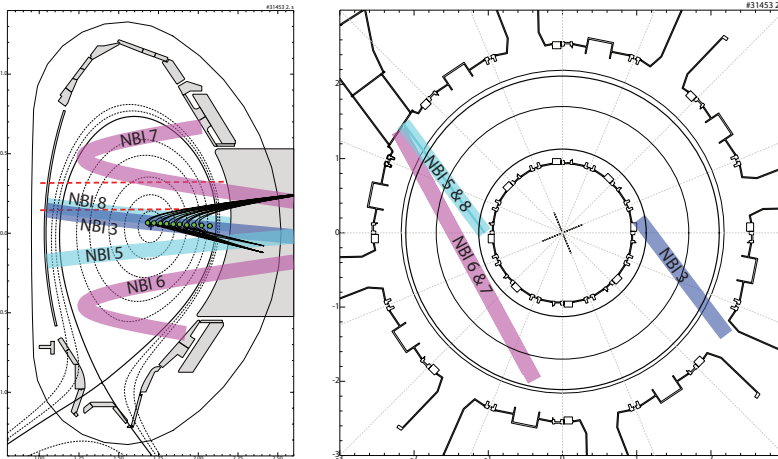


FIG. 1: Left: Poloidal projections of NBI beams geometries (thick transparent lines), Faraday polarimetry lines of sight (dashed, red lines), MSE intersection points with beam 3 (green circles), and FIDA lines of sight (black lines). Right: Toroidal view of the NBI beam geometries.

profile were not in agreement with theoretical predictions [1]. Subsequently these discrepancies were explained by microturbulent radial transport of the fast beam ions with a diffusion coefficient of $\sim 0.5 \text{ m}^2/\text{s}$ [2].

These results triggered a series of investigations on a number of machines [3] and many – though not all – of these experiments confirmed anomalous fast ion (FI) transport during off-axis NBCD. More recently, based on experiments using DIII-D’s new tiltable off-axis neutral beam injector, Pace et al. [4] concluded that anomalous FI transport is negligible under any conditions in DIII-D, revising earlier conclusions from experiments in which the plasma had been shifted vertically to change between on- and off-axis NBCD [5].

The differences in conclusion about the importance of anomalous transport for on- and off-axis NBCD led us to experimentally revisit the problem on ASDEX Upgrade. The discharges again switch between on- and off-axis NBCD to induce transient changes in the radial FI and current profiles. These changes are monitored by the fast-ion D_α (FIDA) and MSE diagnostics. Due to a modified setup of the discharges with respect to the original experiments, MSE and FIDA measure simultaneously and continuously as long as NBI is on [6, 7]. The expected data of the diagnostics are then forward modelled based on TRANSP simulations and the level of anomalous FI transport is estimated by assuming different FI diffusion coefficients in the transport simulations.

In the present paper we focus on the assessment of the errors and sensitivity of the analysis.

2 Instrumentation, Modelling and Improvements

The NBI system features two NBI boxes with four neutral beams each that differ in injection geometry. Two of the beams of box 2 inject toroidally and off axis for effective off-axis NBCD. Every single beam delivers up to 2.5 MW at a beam energy of 60 keV on box 1 and 93 keV on box 2. The neutral-beam-dependent MSE and FIDA diagnostics use beam 3 of box 1.

As the FI distribution function is sensitive to the actual beam injection geometries, they have to be precisely known for the simulations to enable meaningful synthetic diagnostics data. Although the nominal injection geometries are well defined, slight misalignment of a source as a whole or the grids with respect to each other may lead to deviations. In order to determine

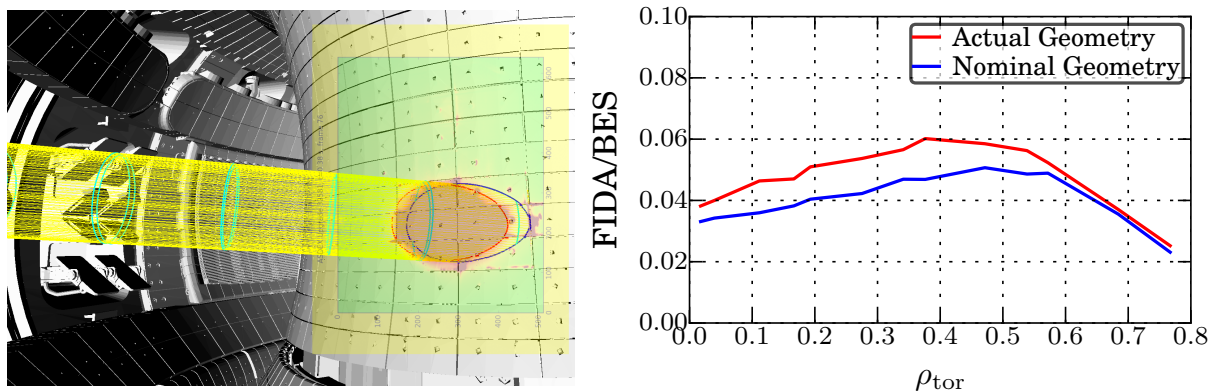


FIG. 2: Left: Example of beam geometry correction for beam 5: The 3D torus model view is overlaid with an infrared image of the beam footprint on the heat shield. The yellow lines visualize the half-maximum-heat-flux-density contour of beam 5 and the red and blue lines its intersection with the heat shield for the corrected and nominal beam geometry, respectively. Right: Influence of the beam geometry correction on synthetic FIDA profiles.

their geometries as precisely as possible the beams of box 2 were fired one by one into the empty torus for short durations for which the first wall can withstand being hit by full NBI power. The resulting local wall heating was monitored with fast infrared (IR) cameras. The images were then overlaid on the corresponding view in a 3D computer model of the torus and compared with the beam intersection contours, as shown in FIG. 2. This led to corrections on the order of 0.1° beam tilting around the source positions. The technique was only applicable to box 2 as suitable IR camera views do not exist for box 1. The significance of the corrections is shown in FIG. 2 by the example of synthetic FIDA data calculated for a phase with beams 3, 6 and 7 with nominal and corrected geometries. The FIDA intensities are visibly different inside $\rho_{\text{pol}} = 0.5$.

MSE [8] measures the polarization of the σ and/or π components of the Stark-split D_α lines of fast NBI neutrals traversing the plasma. This Stark splitting is caused by the Lorentz electric field \vec{E}_L that the magnetic field gives rise to in a frame of reference that moves with the beam neutrals. The σ and π components are polarized perpendicular to each other and the π components are polarized parallel to \vec{E}_L . Hence, MSE allows to determine the local pitch angle of the magnetic field lines (or a projection thereof). The MSE system on AUG uses NBI beam 3 and its lines of sight are shown in FIG. 1.

In practice a number of other effects influence the measured polarization, besides the difficulty of providing absolute reference angles due to the often complex geometries of the setup. Therefore, MSE systems often yield only relative measurements but no absolute angles. These issues have recently been addressed systematically on AUG [9], roughly following the procedures in [10]. For every line of sight its offset was determined by measuring a light source of known polarization. Secondly, nonlinearities in the relationship between actual and measured angle were determined by measuring the instrument function with a full 360° turn of a polarized light source. Thirdly, all optical components in the beamline exposed to the magnetic field can contribute to the measured polarization by Faraday rotation. This effect was quantified by measuring a polarized calibration lamp at various magnetic fields, the result being in perfect

agreement with calculations. As some of the corrections are not simply a shift by a constant offset they are of relevance also for relative measurements. With all current calibrations and corrections applied the remaining systematic errors are of the order of 1° . An in-vessel calibration system is currently being developed to eliminate also these. Another remaining problem is polarized background light from the plasma edge. A planned MSE upgrade with polychromators for each channel will solve this problem by measuring the polarization of the background at slightly shifted wavelengths outside the Stark lines [10, 11]. However, the discharges discussed below had no pronounced background light contribution.

Other diagnostics relevant for this study are the loop voltage measurement, FIDA, and, in principle, Faraday polarimetry. Faraday polarimetry is installed on two of the radial lines of sight (see FIG. 1) of the DCN interferometer. It is generally sensitive to changes of the current profile, but modelling predicts little sensitivity to moderate fast ion diffusion. Therefore we do not further discuss this diagnostic here. The Fast Ion D_α spectroscopy (FIDA) [12] measures the intensities of the Doppler shifted D_α light emitted by fast (usually neutral-beam-injected) ions after being neutralized upon crossing a neutral beam by charge exchange with a beam neutral. It thus provides a radial intensity measurement of the fast ions in the accessible pitch angle and energy range. The lines of sight are indicated in FIG. 1. Finally, loop voltage measurements contain information on the inductively driven current. If all relevant quantities such as Z_{eff} , T_e and n_e profiles are known with sufficient accuracy, loop voltage measurements can also be exploited to infer the non-inductively driven current.

Transport and NBCD modelling is carried out using TRANSP/NUBEAM. For all of the mentioned diagnostics synthetic data are then calculated by post-processing the TRANSP output, e.g. using FIDASim [13] to calculate the expected FIDA spectra and intensity profiles. Different levels of anomalous transport can be simulated by providing TRANSP with anomalous diffusion coefficients.

3 Anomalous Transport

FIG. 3 shows an overview of a typical on/off-axis NBCD discharge (#32148). NBI beam 3 is continuously on to enable FIDA and MSE with the exception of short notches for background measurements. The discharge starts with two additional on-axis neutral beams that are replaced by the two off-axis beams between 4.5 and 7.0 s. ECRH gyrotron 5 provides central co-ECCD for sawtooth suppression, gyrotron 8 is used for preemptive NTM stabilization at the $q = 3/2$ surface, gyrotron 7 is used for central electron heating, and the T_e -feedback-controlled gyrotron 6 compensates for the loss of central electron heating when switching NBI from on to off axis, resulting in remarkably constant T_e and n_e profiles. MHD activity is limited to fishbones in the on-axis phases and sawteeth with a period of 200–250 ms in the first on-axis phase. The depicted on-axis FIDA measurements correspond to a time point before a sawtooth crash.

FIG. 4a) presents the calibrated (unshifted) MSE angles measured by four different lines of sight (black) at major radii between 1.73 and 1.94 m (the magnetic axis is at 1.7 m and the separatrix position at the outer midplane is at 2.1 m). Also shown are three different simulations from neo-classical transport only to an anomalous fast ion diffusion coefficient of $D_{\text{fi}} = 0.5 \text{ m}^2/\text{s}$. There are three important observations: (1) All simulations do practically coincide in the off-

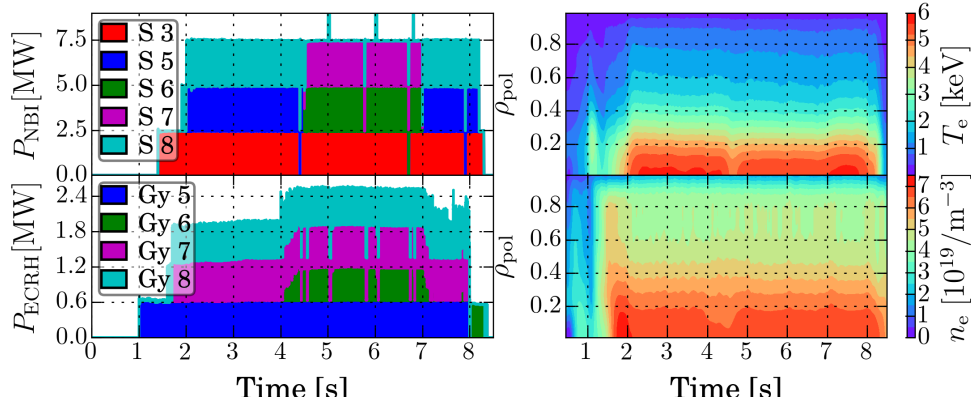


FIG. 3: Overview of discharge #32148. Top left: NBI power with color coded beam assignment. Bottom left: ECRH power with color coded beam assignment. Top right: Color map of the time-dependent T_e profile. Bottom right: Color map of the time-dependent n_e profile.

axis phase. In other words, the MSE system is not sensitive to realistic levels of anomalous transport and cannot answer the question that initially served as a motivation for these studies. (2) In the on-axis phase differences with D_{fi} are visible, but comparable with the noise of the MSE angles of about 0.2° and hence too small to be resolved. (3) As the differences are visible only in the on-axis phase, absolute calibration of the MSE angles provides no additional information, because the relevant information is also in the step height at the transition from on to off axis and vice versa. However, the removal of nonlinearities of the angle measurement achieved by the calibration is also of relevance for the relative changes of the angles.

Similar conclusions can be reached from the FIDA profiles. The FIDA intensity profiles in FIG. 4b) and c) are normalised to the local beam emission (BES) intensity in order to present data that are closer to the radial fast ion density profile in the accessible phase space region. Again, simulations in the off-axis phase with different D_{fi} are almost identical and in reasonable agreement with the data. However, as opposed to MSE, FIDA can resolve the differences in D_{fi} in the on-axis case and best agreement with the data is achieved with D_{fi} between 0.1 and 0.3. **The additional simulation shown in magenta assumed an energy-, time-, and ρ -dependent diffusion coefficient calculated according to Pueschel et al. [14]. This simulation is also in reasonable agreement with the data. (TRANSP sim. still pending)**

The reason why both FIDA and MSE are so relatively sensitive to anomalous fast-ion transport in the on-axis, but not the off-axis phase, can be intuitively understood from FIG. 4: In the on-axis case the fast-ion density and current profiles are centrally peaked and moderate diffusion flattens them considerably, while in the off-axis case the profiles are already flat and diffusion leads to little change. This is aggravated by the continuous presence of beam 3 in our discharges as opposed to the original off-axis-current-drive experiments [2]. In these experiments the fast-ion profiles must have been somewhat hollow which means there may be more effect of fast-ion transport on FIDA and MSE. This still needs to be reviewed.

Interestingly simulations of the loop voltage assuming different D_{fi} do show differences in the off-axis case, albeit not sufficient to be resolved experimentally given the large excursions in

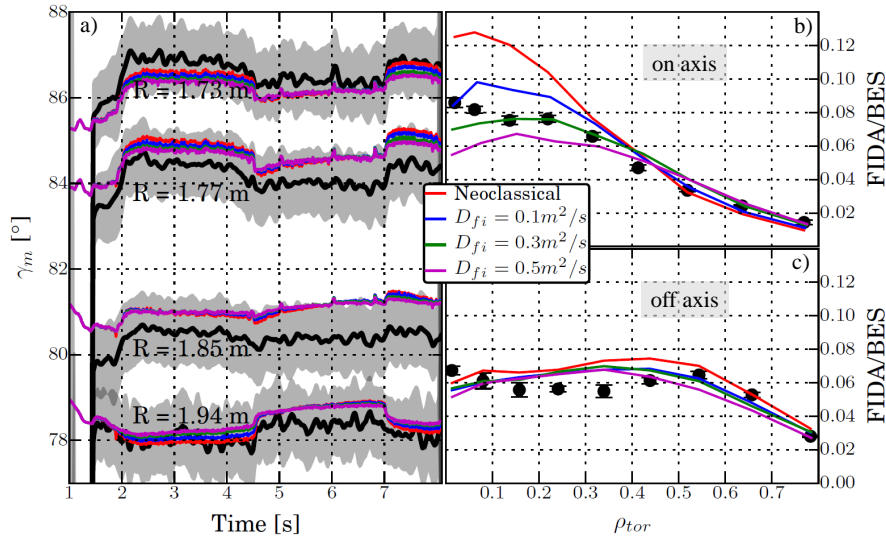


FIG. 4: a) MSE data for discharge #32148 (raw in gray and filtered in black) and synthetic MSE data from TRANSP simulations assuming only neoclassical transport (red) and fast ion diffusion coefficients of 0.1 (blue), $0.3 \text{ m}^2/\text{s}$ (green), and $0.5 \text{ m}^2/\text{s}$ (purple). b) FIDA profiles for discharge #32148 and comparison with simulations assuming different anomalous fast-ion diffusion coefficients during on-axis phase at 4.33 s and c) off-axis phase at 6.60 s.

the measured loop voltage. This can be understood as follows: FIDA measures a local fast-ion density that does not change very much if anyway flat profiles are subject to diffusion. MSE at minor radius r measures a change in the local pitch angle that depends on the total toroidal plasma current inside $\rho(r)$. Little changes of the NBCD profile lead to negligible changes of this current, especially when the total current is kept constant. On the contrary, the loop voltage is proportional only to the inductively driven current. When the NB driven current changes and assuming that the other non-inductive contributions stay constant, this change is compensated by an opposite change of the inductive current that, if large enough, can be measured.

4 Absolute Current Drive Efficiency and Completely Non-Inductive Discharges

In order to achieve a high non-inductive current fraction, scenarios were run in which the simultaneous maximization of neutral beam driven and bootstrap current was attempted [15] (see also J. Stober et al., this conference). The primary means to achieve this were high T_e , low n_e , and a hollow current profile. High T_e was primarily obtained by β_{pol} feedback control using the NBI power as actuator to operate as close as practically possible to the stability limit. The hollow current profile in the center was produced through placing most of the externally driven current off axis by preferential use of the off-axis neutral beams and appropriate ECH launcher angles.

The most relevant time traces of the discharge are shown in FIG. 5. Starting from 1.2 s

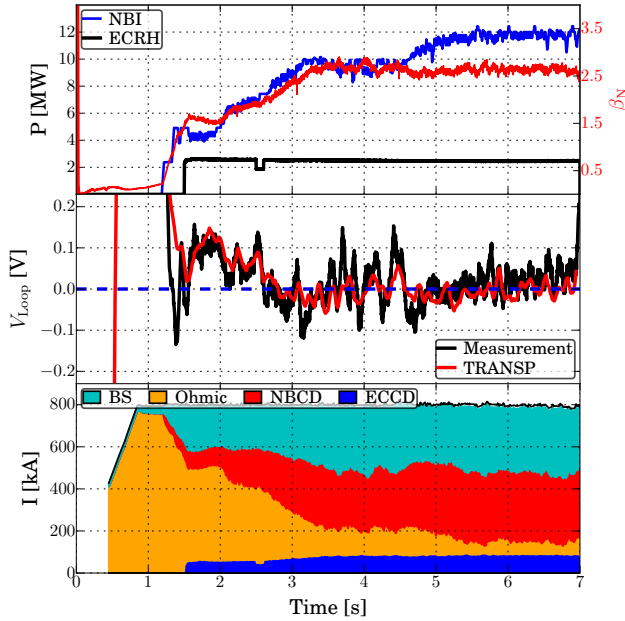


FIG. 5: Overview of the non-inductive discharge #33134: Top: NBI power, ECRH power, and β_N . Center: Measured and TRANSP-calculated loop voltage. The current in the central solenoid was set to constant from 4.5 s onwards. Bottom: Measured plasma current (black) and current composition as calculated by TRANSP with bootstrap current in red, ohmic (inductive) current in orange, neutral beam driven current in cyan, and EC driven current in blue.

the NBI power is gradually increased to follow a pre-programmed β_{pol} ramp that results in a final $\beta_N \sim 2.5$. At around 4.5 s a 3/2 NTM appears and more NBI is required henceforth to keep β_{pol} at the desired level. Constant ECH is also applied and driving current in co-current direction. From 4.5 s onwards the current in the central solenoid is set constant to prevent any further inductive current drive. However, inductive current created before that time has not been substituted by other contributions may still be present and decay on a resistive time scale of the order of multiple seconds. The measured loop voltage and that predicted by TRANSP is shown in the center panel. Both signals remain very close to zero after 4.5 s in line with little to no inductive current drive. The good agreement between measured and calculated loop voltage over the entire discharge confirms the high accuracy of the Z_{eff} profiles calculated from absolute impurity densities measured with charge exchange spectroscopy, rendering loop voltage measurements a reliable diagnostic for inductively driven current.

The bottom panel in FIG. 5 shows the total plasma current I_p in black and the different constituents as calculated by TRANSP. After 4.5 s I_p stays practically constant without further inductive current drive, implying that the inductive current is close to zero. The TRANSP analysis predicts that most of the current during this phase is driven by BS and NBCD with $> 40\%$ each while ECCD and inductive current contribute $\sim 8\%$ each. It has to be noted that TRANSP calculates the inductive current as the difference between I_p and the non-inductive contributions. This consistency of experiment with simulation also provides a good benchmark for the modelled total neutral beam driven current, suggesting that it is not far off.

5 Conclusions

Although the initial aim of revisiting the on-/off-axis NBCD experiments had been to investigate anomalous fast ion transport in the off-axis phase, it turns out that the available diagnostics,

although forming a comprehensive set and being state of the art, are not sensitive enough to answer this question on AUG with the current set of experiments. On the contrary, during on-axis NBI with its centrally peaked fast ion profiles FIDA is sensitive to anomalous transport with diffusion coefficients as low as $0.1 \text{ m}^2/\text{s}$. In the discharge presented here in fact about $0.2\text{--}0.3 \text{ m}^2/\text{s}$ are needed to describe the data, although a contribution of fishbone activity cannot be ruled out for this discharge.

The practically non-inductive discharge presented here allows quantitative benchmark of the TRANSP/NUBEAM calculated NB-driven current, suggesting it is not far off.

6 Acknowledgement

This work has been carried out within the framework of the EUROfusion Consortium and has received funding from the Euratom research and training programme 2014–2018 under grant agreement No 633053. The views and opinions expressed herein do not necessarily reflect those of the European Commission.

References

- [1] J. Hobirk et al., Proc. 30th EPS Conf. Contr. Fusion Plasma Phys., Vol. 27A (2003) O-4.1B.
- [2] S. Günter et al., Nucl. Fusion 47 (2007) 920.
- [3] T. Suzuki et al., Nucl. Fusion 51 (2011) 083020.
- [4] D. C. Pace et al., Phys. Plasmas 20 (2013) 056108.
- [5] W. Heidbrink et al., Phys. Rev. Lett. 103 (2009) 175001.
- [6] B. Geiger et al., Plasma Phys. Control. Fusion 57 (2015) 014018.
- [7] B. Geiger et al., Nucl. Fusion 55 (2015) 083001.
- [8] R. Wolf et al., J. Instr. 10 (2015) P10008.
- [9] A. Bock et al., Proc. 43rd EPS Conf. Plasma Phys., 2016.
- [10] R. T. Mumgaard et al., Rev. Sci. Instrum. 85 (2014) 053505.
- [11] R. T. Mumgaard, Ph.D. thesis, Massachusetts Institute of Technology (2015).
- [12] B. Geiger, Ph.D. thesis, Ludwig-Maximilians-Universität München (2013).
- [13] W. Heidbrink et al., Commun. Comput. Phys. 10 (2011) 716.
- [14] M. J. Poeschel et al., Nucl. Fusion 52 (2012) 103018.
- [15] A. Bock, Ph.D. thesis, Ludwig-Maximilians-Universität München (2015).